



## Analysis of sensors used for interaction-based condition assessment of concrete

C. (Catalin) Cernat

BSc Report

**Committee:**

H. Noshahri, MSc  
dr.ir. E. Dertien  
dr.ir. L.L. Olde Scholtenhuis

July 2019

028RAM2019  
Robotics and Mechatronics  
EE-Math-CS  
University of Twente  
P.O. Box 217  
7500 AE Enschede  
The Netherlands



## Preface

I would like to start by saying that undertaking this bachelor assignment within the RaM department strengthened my convictions and interests in robotics. While writing my bachelor thesis i realized that indeed, this is the path i would like to follow as a future study and career. This is mostly due to the friendly and open environment within the RaM department and to my daily supervisor who showed me how beautiful the academic research can be.

I would like to express my special gratitude of gratitude to my supervisors and committee members H. Noshahri, MSc, dr.ir. E. Dertien and dr.ir. L.L. Olde Scholtenhuis for all the support offered on my journey of writing this bachelor thesis. Their supportive and positive attitude made my stay within the RaM department a very pleasant one. Furthermore, i would like to show my sincere appreciation to the secretary, J.M. Boelema - Kaufmann and all the technical staff who were very responsive, helpful and oriented to the student's needs.

Lastly i would like to thank my friends and family who always supported, encouraged and motivated me through my bachelor study and while writing this thesis.

Catalin Cernat  
Enschede, 28 June 2019



---

# Contents

<b>1 Introduction</b>	<b>1</b>
1.1 Context . . . . .	1
1.2 Research goal . . . . .	1
1.3 Thesis outline . . . . .	1
<b>2 Analysis</b>	<b>3</b>
2.1 Impact-echo method . . . . .	3
2.2 Sensing . . . . .	7
2.3 Data processing . . . . .	9
2.4 Influence of disturbances . . . . .	10
2.5 Chapter summary . . . . .	10
<b>3 Design</b>	<b>11</b>
3.1 Setup description . . . . .	11
3.2 Test scenarios . . . . .	13
3.3 Method . . . . .	14
<b>4 Results and discussion</b>	<b>15</b>
4.1 Time domain response . . . . .	15
4.2 Signal to noise ratio . . . . .	16
4.3 Frequency spectrum using FFT . . . . .	17
4.4 Time development of thickness frequency using STFT . . . . .	19
<b>5 Conclusion and recommendations</b>	<b>23</b>
5.1 Conclusion . . . . .	23
5.2 Future work . . . . .	24
<b>A Appendix 1</b>	<b>25</b>
<b>Bibliography</b>	<b>26</b>



# 1 Introduction

With the increasing size of the cities, the underground sewage infrastructure that supports them becomes more complex. Maintenance and inspection routines become harder to execute and the multi-layer structure makes it difficult to access certain parts which must be evaluated. Nowadays, the assessment of concrete sewage systems is performed using CCTV cameras and inspecting the captured images for defects. This limits the evaluation only to flaws that are visible at the inner surface of the sewers.

## 1.1 Context

The research is being done in the context of TISCALI (Technology Innovation for Sewer Condition Assessment using Long-distance Information-system) project as an effort to provide meaningful insights regarding different sensing methods. The primary objective of the TISCALI project is to determine the constructive strength and stability of sewers using an in-pipe inspection robot. The robot uses the impact-echo method to excite the sewer with a prescribed energy and for a certain duration by the means of an impactor developed in Robotics and Mechatronics (RaM) group. A sensor is used to record the response of the structure to the applied impulse.

## 1.2 Research goal

The goal of this bachelor assignment is to analyze and to compare the signals recorded by various sensors which are developed for vibration or acoustic signal measurement. The outcome of this assignment will help determining the most suitable sensor to be mounted on the in-pipe robot which will enable contactless assessment of the concrete structure. Laboratory experiments will be conducted using impact-echo method. For this purpose, concrete tiles(plates) will be used as samples instead of a full scale sewer pipe. Furthermore, the research is taken one step further in an attempt to detect the presence of a void in the support substrate, since CCTV inspection can not identify this type of flaws. The study will focus on comparative measurements between concrete plates with a damaged substrate and undamaged substrate. To this extent, more specific research questions must be answered thoroughly:

- How is a void under a concrete plate discovered using impact-echo method?
- How do material properties(density and Poisson's ratio) of the concrete tile affect the impact-echo response?
- How can the measured data be processed to determine the presence of a flaw in the support substrate, underneath the concrete plates?
- How do sensors compare to each other for the detection of the impact-echo response and the state of the substrate?

## 1.3 Thesis outline

First chapter provides an introduction to the topic alongside the research goal and an outline of the thesis. Second chapter shows an overview of the theoretical background needed to understand the working principle of assessing the state of the concrete and its substrate. It includes a description of each sensor that can be used to perform the measurements alongside data processing techniques. Third chapter describes the available setup and the procedure that is going to be followed to perform the measurements. The fourth chapter presents the time waveforms recorded together with all the results and discussion necessary to draw a final conclusion. Last

chapter concludes the thesis by presenting answers to the research questions and an overall conclusion of the results alongside recommendations for future work.

## 2 Analysis

Although the study focuses on investigating different sensing devices using impact-echo method, the impact generation will be described as well since it plays a key role in receiving the correct response from the concrete plates.

### 2.1 Impact-echo method

Impact echo method, as stated by Sansalone (12), had an early success as a Non Destructive Technique(NDT) for assessing the state of the the concrete and detecting flaws within the structure. A basic setup can be seen in figure 2.1.

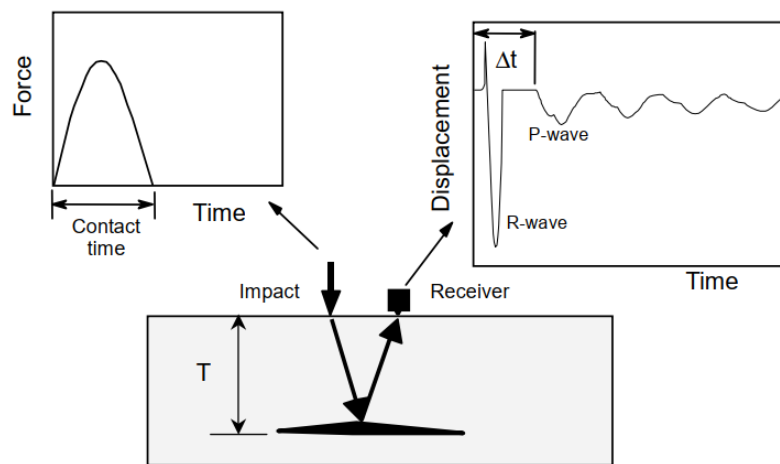


**Figure 2.1:** Impact-echo method basic setup (Carino et al. (3))

The working principle of this method is based on creating stress waves within the material. As stated in Carino et al. (3) when there is a sudden disturbance at a certain point on the surface of a solid material, three different types of stress waves can be distinguished: Rayleigh waves, which propagate along the surface and away from the impact point, Secondary(S) waves which propagate due to the shear stress and Primary(P) waves which propagate due to the normal stress. At a certain point on the surface, the resulting wave motion generates acoustic waves called leaky waves that propagate into the surrounding fluid (Zhu and Popovics (13)). The P waves frequency is dependent on the thickness of the solid material and it would be referred to as the thickness frequency.

The speed of the P wave( $C_p$ ) can be calculated as it follows(assuming an infinite, isotropic and elastic solid)(Krautkrämer and Krautkrämer (7)):

$$C_p = \sqrt{\frac{E(1-\nu)}{\rho(1+\nu)(1-2\nu)}} \quad (2.1)$$

where  $E$  is Young's modulus of elasticity,  $\rho$  is the density of the solid and  $\nu$  Poisson's ratio.

However, another study showed that the speed of the wave( $C_{pp}$ ) related to the thickness frequency is only 96% of the actual P wave speed in equation 2.1( Lin and Sansalone (8)).

Based on the thickness of a concrete plate and the known thickness wave speed( $C_{pp}$ ), the frequency at which the response is expected can be calculated as it follows (Carino et al. (3)):

$$f_t = \frac{C_{pp}}{2T} \quad (2.2)$$

where  $T$  is the thickness of the concrete plate.

To excite the thickness frequency of a concrete tile of specific thickness, a simple method can be used. By allowing a steel ball to fall freely from a certain height, the required impact can be created. Colla and Lausch (4) showed that the maximum frequency that a steel ball can excite depends only on the diameter of the ball. The following equations can be used to determine the minimum diameter( $D$ ) of the steel ball:

$$t_c = 0.0043D \quad (2.3)$$

where  $t_c$ (s) is the contact time between the ball and the medium and  $D$ (m) the diameter of the steel ball.

$$f_{max} = \frac{1.25}{t_c} \quad (2.4)$$

where  $f_{max}$ (Hz) is the maximum frequency of the waves that a steel ball can excite.

Finally, substituting equation 2.3 in equation 2.4, the diameter of the ball with respect to  $f_{max}$  can be calculated as it follows:

$$D = \frac{291}{f_{max}} \quad (2.5)$$

Furthermore, knowing that  $f_{max}$  must be higher than the thickness frequency( $f_t$ ) (Carino et al. (3)), the minimum diameter of the steel ball with respect to the concrete thickness can be calculated as it follows:

$$D = \frac{291}{f_t} = \frac{291}{\frac{C_{pp}}{2T}} = \frac{582T}{C_{pp}} \quad (2.6)$$

Theoretical estimations of the diameter of the ball for concrete plates with different thicknesses have been performed and can be seen on the right axis of figure 2.2. On the left axis of figure 2.2 the expected thickness frequency is displayed. In order to excite the waves with these frequencies within a concrete plate with a thickness of 40mm(the thinnest available in the lab) a steel ball of 6.7mm diameter is sufficient. This can be seen in figure 2.2.

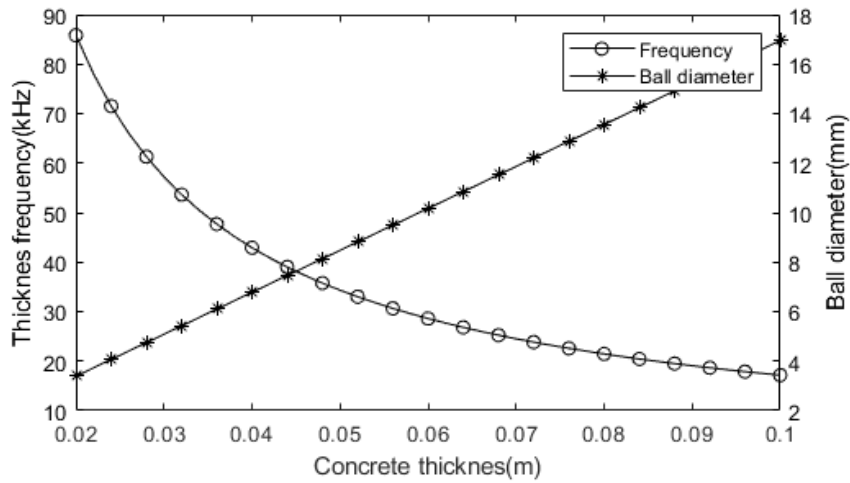


**Figure 2.2:** Thickness frequency and ball diameter vs. concrete thickness (for Poisson's ratio=0.16 and concrete density of  $2300\text{kg}/\text{m}^3$ )

### 2.1.1 Material properties

As the composition of concrete can vary depending on the manufacturer and on the recipe used, the influence of Poisson's ratio and of concrete density has been investigated. Using equation 2.1, for a concrete plate of  $80\text{mm}$  thickness and a fixed density of  $2300\text{kg}/\text{m}^3$ , the change in thickness frequency can be seen in figure 2.3. Poisson's ration has been swept from 0.1 to 0.2 with increments of 0.01.

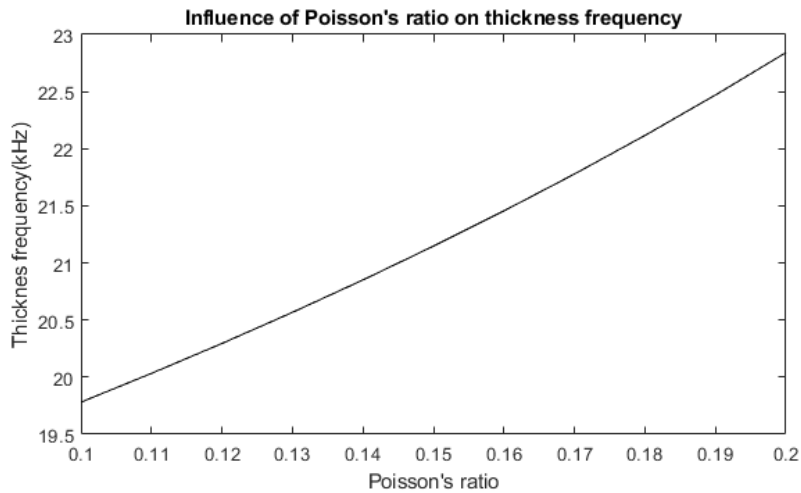


**Figure 2.3:** Thickness frequency vs. Poisson's ratio (thickness= $80\text{mm}$  and concrete density of  $2300\text{kg}/\text{m}^3$ )

Besides Poisson's ratio, as can be seen from equation 2.1, the density of the concrete also influences the P wave speed which in turn results in variations of the thickness frequency. For a plate thickness of  $80\text{mm}$  and a Poisson's ratio of 0.16, the density of the concrete has been swept from  $1900\text{kg}/\text{m}^3$  to  $2300\text{kg}/\text{m}^3$  with increments of 1 (Dorf and Richard (5)). The change in thickness frequency can be seen in figure 2.4

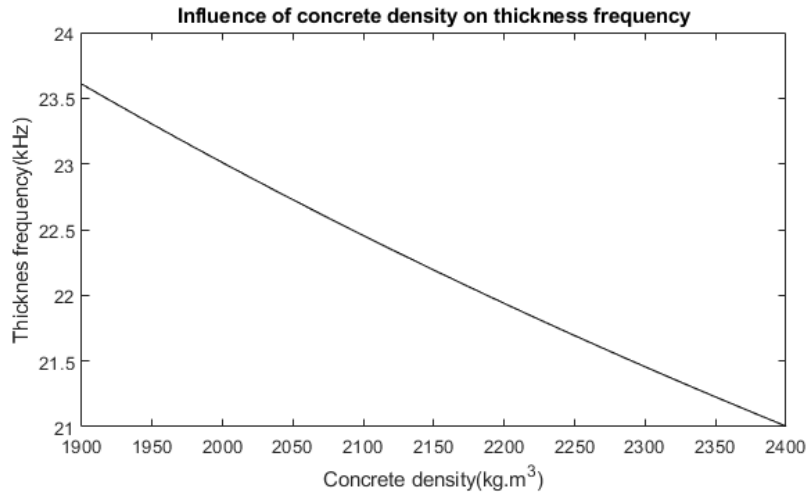


**Figure 2.4:** Thickness frequency vs. density (thickness=80mm and Poisson's ratio=0.16)

The aforementioned calculations have been performed based on the assumption that there is no direct correlation between Poisson's ratio and density of the concrete. This aspect has not been investigated further as it is out of the scope of this research paper.

### 2.1.2 Specific acoustic impedance

Specific acoustic impedance represents the product between the density and the speed of the wave propagating through a material. When a wave, traveling through a material arrives at the interface between the first material and the second material, a part of the incident wave is reflected. For normal incidence,  $R$ , the reflection coefficient is given by (Krautkrämer and Krautkrämer (7)):

$$R = \frac{Z_2 - Z_1}{Z_2 + Z_1} \quad (2.7)$$

where  $Z_1$  is the specific acoustic impedance of the first material and  $Z_2$  is the specific acoustic impedance of the second material, as shown in figure 2.5

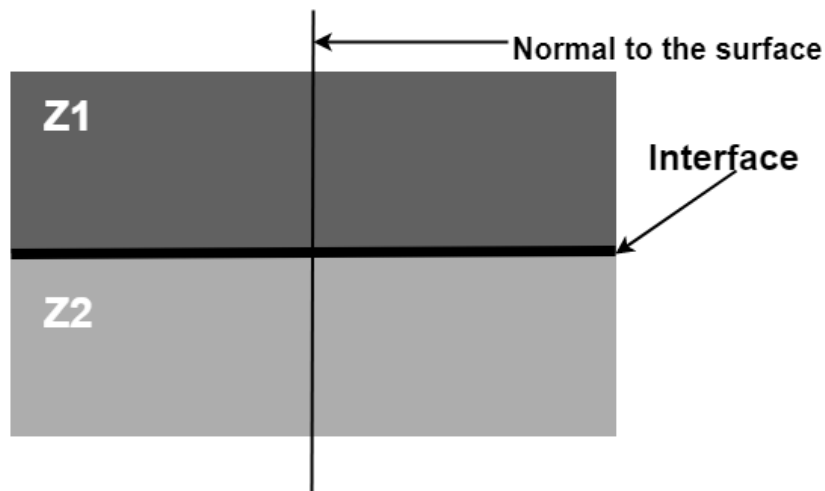


**Figure 2.5:** Two dissimilar materials and the interface in between

When  $|R| = 1$  the wave is totally reflected and when  $|R| = 0$  the wave is absorbed by the material coming after interface. This principle is used when analyzing the temporal trace of the waves excited within a concrete plate. Calculations have been performed for the reflection coefficient, for two scenarios: concrete-air and concrete-soil. A median specific impedance of  $8 \cdot 10^6 \text{ kg}/(\text{m}^2 \text{ s})$  and  $0.4 \text{ kg}/(\text{m}^2 \text{ s})$  for concrete, respectively air have been obtained from (Carino et al. (3)).

$$|R_{\text{concrete-air}}| = \left| \frac{0.4 - 8 \cdot 10^6}{0.4 + 8 \cdot 10^6} \right| = 0.999 \quad (2.8)$$

$$|R_{\text{concrete-soil}}| = \left| \frac{2 \cdot 10^6 - 8 \cdot 10^6}{2 \cdot 10^6 + 8 \cdot 10^6} \right| = 0.6 \quad (2.9)$$

When a concrete tile lies directly on a soil(during the experiments for this thesis sand) substrate, the reflection coefficient is lower than when there is a cavity filled with air in the substrate. In turn, since  $|R_{\text{concrete-air}}| > |R_{\text{concrete-soil}}|$ , the temporal trace of the excited waves will last longer for a substrate with a cavity than for a substrate with no cavity at all.

Material	Specific acoustic impedance, $\text{kg}/(\text{m}^2 \text{ s})$
Air	0.4
Water	$0.5 \times 10^6$
Soil	$0.3 \text{ to } 4 \times 10^6$
Concrete	$7 \text{ to } 10 \times 10^6$
Steel	$47 \times 10^6$

**Figure 2.6:** Specific acoustic impedance for certain materials(Carino et al. (3))

## 2.2 Sensing

Two sensing methods can be distinguished:

- Contactless(air coupled) - There is a distance between the sensor and the surface which has to be measured therefore, the sensor does not touch the surface
- Contact sensing(surface coupled) - The sensor is in direct(or through another medium, like wax) contact to the surface that has to be measured

As the main objective is to mount the sensors on an in-pipe robot, air coupled sensors are preferred over surface coupled ones. Furthermore, an important parameter that one must pay attention to is the bandwidth of the sensors. As can be seen in figure 2.2, the sensors must be able to sense frequencies up to 43kHz.

### 2.2.1 Vibration accelerometer

Charge mode accelerometers are designed to measure vibrations and shocks. Their output is a high impedance electrical signal which is directly proportional to the applied acceleration. Since their direct output is not amplified, low noise cable and charge amplifiers must be used to ensure that the output data is readable on general purpose instrumentation.

Brüel & Kjær type 4374 vibration accelerometer is used and has a charge sensitivity of  $1.47 \text{ pC}/g$ . It has a bandwidth of 26kHz with constant sensitivity. Afterwards, the sensitivity increases, reaching its peak around 85kHz. This can be seen in figure 2.7 (Brüel & Kjær (2)).

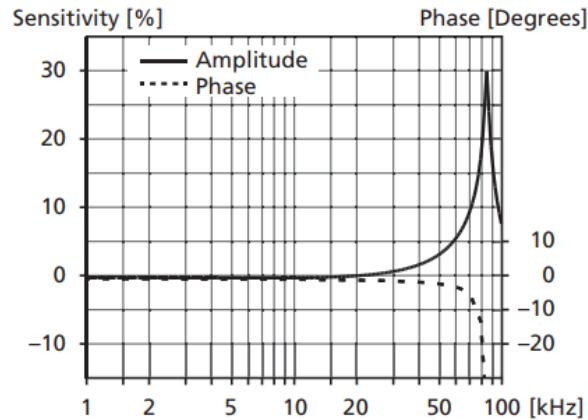


Figure 2.7: Accelerometer sensitivity vs. frequency (Brüel & Kjær (2))

### 2.2.2 Microphone

Microphones can be used to measure leaky surface waves as shown by Ryden et al. (11) and are suitable for assessing the state of concrete plates. Furthermore, Zhu and Popovics (13) showed that a regular microphone with a sensitivity of only  $4\text{ mV}/\text{Pa}$  (measured at 1000Hz and 94dB) can be used to measure the leaky surface waves.

Behringer ECM8000 measurements microphone is used and has a sensitivity of  $11\text{ mV}/\text{Pa}$  (measured at 1000Hz and 94dB). The microphone has constant gain up to a frequency of 20kHz, then it decays to -10dB for frequencies of 30kHz at a rate of 20dB per octave. This can be seen in figure 2.8 (Behringer (1)).

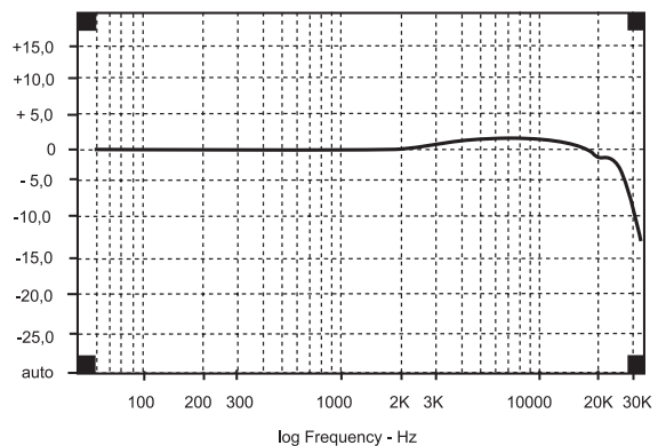


Figure 2.8: Microphone sensitivity vs. frequency (Behringer (1))

### 2.2.3 Laser vibrometer

A laser vibrometer uses laser interferometry to precisely determine velocity and displacement of structures. Light scattered by moving objects changes its frequency slightly. The interferometer detects those slight changes of the back scattered light, revealing the Doppler shift in frequency. As mentioned by Zhu and Popovics (13), the application of laser in this context is limited by the rough surface of concrete.

Polytec OFV-5000 controller and Polytec OFV-505 laser head have been used and together they have a bandwidth 2.5MHz and a typical sensitivity of  $0.02\mu/s$ , as shown in the datasheet (Polytec (10)).

### 2.2.4 Particle velocity sensor

A particle velocity sensor, developed at University of Twente uses two hot platinum wires. When air particles move around the two wires, the temperature distribution changes and so, the speed of the particles can be measured.

Microflown PU regular particle velocity sensor is used and has a bandwidth limited to 20kHz with the correction feature on. Otherwise the sensor has a bandwidth of only 10kHz. After the 20kHz threshold, for frequencies of 30kHz, the sensitivity decreases by a factor of  $7 \cdot 10^{-3}$ . This can be seen from figure 2.9 (Microflown Technologies).

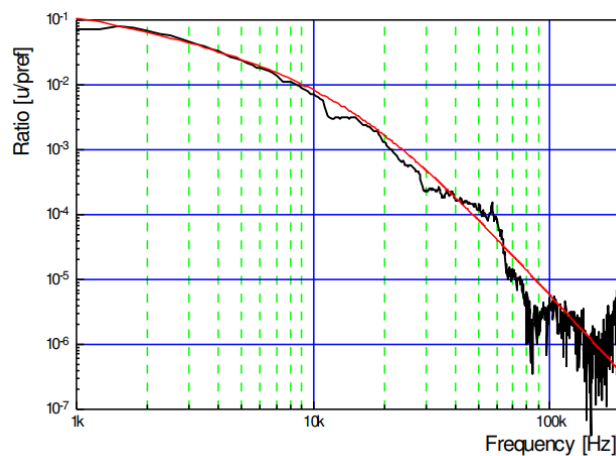


**Figure 2.9:** Particle velocity sensor sensitivity vs. frequency (Microflown Technologies)

## 2.3 Data processing

### 2.3.1 Preprocessing

The signal to noise ratio(SNR) is a measure of how good a signal can be distinguished compared to the noise present at that time. To accomplish this, a sample containing noise and a sample containing the signal and the noise are needed. The SNR will aid in the decision making process when the most suitable sensor to be mounted on the robot will be chosen.

As stated in section 2.2, the sensors used have different sensitivity and in turn, all the data that is measured has to be normalized such that a common scale is reached. This procedure is called normalization of ratings.

Digital filtering is used to remove unwanted interferers from a signal as well as narrowing the response to a region of interest. It represents an important step towards reaching the goal of the thesis since sensors that can pick up sound waves within the audible range are being used for performing measurements

### 2.3.2 Fast Fourier Transform(FFT) and Short Time Fourier Transform(STFFT)

After the data is acquired, Fourier Transform will be used to create a frequency vs. amplitude plot and determine the thickness frequency. However, this does not give any information about the temporal variations of the frequency spectrum. For this, short time Fourier transform(STFFT) will be used. STFFT uses FFT to analyze the frequency content of short

part(window) of the original signal. Afterwards, the window is shifted by a certain amount of samples and FFT is used to evaluate the frequency content again. The process continues until the end of the data sample is reached. As reported by Kang et al. (6), a spectrogram would be the best way to visualize the results of STFT vs. time since a damaged substrate induces longer trails in the spectrogram due to higher specific acoustic impedance contrast.

## **2.4 Influence of disturbances**

As the sensors must be mounted on an in-pipe robot, in that context, there can be various sources of external disturbances, based on which type of sensor is used. If a microphone is used, sound generated by moving parts of the robots and other human activities can influence the measurements. On the other hand, due to the high sensitivity of the laser vibrometer, a perfectly stable mounting mechanism is needed to ensure proper measurements, otherwise the simple fact of hanging the sensor above the surface can influence the measurements drastically. Regarding the particle velocity sensor, wind and particle movement generated by slight shifts of the mechanism of the robot can induce a DC bias in the output reading of the sensors.

Furthermore, as the robot will be connected to power, there is no need to worry about the consumption of each sensor or equipment necessary to perform the measurements. However, the size of the sensors play an important role. As the robot might need to be able to move in confined spaces, a small form factor would be preferred. As stated by the manufacturer, both the particle velocity sensor and the laser vibrometer can be miniaturized to a certain degree. The sensor that can achieve the highest degree of miniaturization is the microphone since MEMS microphones have, in general, smaller form factor compared to measurement microphones.

## **2.5 Chapter summary**

Impact echo method can be used to generate waves with specific frequencies within a concrete tile. In order to excite the right frequency, an impactor(a steel ball in this case) with a diameter of at most 6mm has to be used. Calculations have been performed and the dependencies of thickness frequency on the thickness of the tile, on the Poisson's ratio and on the density of the concrete have been shown. Having in mind the fact that a wave can be reflected or absorbed at an interface of two dissimilar materials, air voids underneath concrete tiles can be detected. Four different sensors, three contactless and one contact reference sensor are used to record the response of the concrete tile after excitation. Finally, the data is first filtered and then processed using FFT and STFT in an attempt to compare the contactless sensors and to find out whether a void underneath a concrete tile can be identified or not.

## 3 Design

### 3.1 Setup description

The test setup consists of a bucket filled with sand. On top of the sand, a concrete sample of 30cm X 30cm and thickness of 80mm is placed. Although thinner concrete tiles are available for testing purposes, only the 80mm thickness one will be used. The reason for this decision is that, as presented in section 2.2, the sensors are not suitable for measuring frequencies higher than 30kHz, except the laser vibrometer. The test concrete tile has a theoretical thickness frequency of 21.45kHz (figure 2.2), thus being suitable for experiments with all sensors. In accordance with the data represented in chapter 2, as an impact generator, a steel ball with a diameter of 6mm will be used since this can be easily found in the lab.

For data acquisition, Rohde&Schwarz RTB2004 oscilloscope has been used and can be seen in figure 3.1 alongside the laser vibrometer setup. It is a four channel oscilloscope and has a maximum sample rate of 2.5 Giga samples per second. However, for the purpose of this thesis, the sample rate has been set to 5 Mega samples per second.



**Figure 3.1:** Laser vibrometer setup - overview of the setup(left) and top view(right)

Besides the laser head, the laser vibrometer needs a controller for the laser head which processes the raw data from the head unit and outputs the velocity to the oscilloscope. This configuration can be seen in figure 3.1 left where the oscilloscope and the laser controller lay on the table while the laser head hangs above the test surface as shown in figure 3.1.



**Figure 3.2:** Microphone setup - overview of the microphone(left) and close up view(right)

The microphone uses an amplifier to deliver the signal to the oscilloscope, however, for this experiment, the gain was set to 0dB since the microphone itself was sensitive enough. As shown in figure 3.2 right, the microphone does not touch the surface, it lays just above the surface at a distance smaller than 1cm. This is due to the very near field effects which won't be analyzed further, as it is out of the scope of this research report.



**Figure 3.3:** Accelerometer setup - type 4374 accelerometer(left) and charge amplifier(right)

As the accelerometer is a contact sensor, it will be used as a reference to compare the other three contactless sensors. In order to make the small structural vibrations of the concrete tile visible, it needs a dedicated charge amplifier which can be seen in figure 3.3 right. Furthermore, to ensure proper transfer of the vibrations from the surface to the accelerometer, it is recommended to use wax as bonding material. This constitutes a big disadvantage if an autonomous in-pipe robot is desired.



**Figure 3.4:** Particle velocity sensor setup - PU regular probe(left) and amplifier(right)

The PU regular probe in figure 3.4 left can sense particle movements in one direction only and in turn, it must be positioned carefully, as close as possible to the surface, without touching it. It needs a custom signal conditioner designed by Microflown (figure 3.4 right) which has two adjustable parameters: the correction factor and the gain. The correction factor ensures a constant gain for frequencies up to 20kHz, but it adds noise to the signal. The gain is not specified and has only two levels: high or low. For the purpose of this experiment, the correction factor was turned on and the gain was set to high.

### 3.2 Test scenarios

To test the sensors, two test scenarios have been created. First, a concrete tile is placed on top of sand substrate. Measurements are performed and afterwards a hole with a volume of approximately  $795\text{cm}^3$  is created within the sand substrate. It is crucial to investigate these two situations because, as stated in section 2.1, the contrast of the specific acoustic impedance between air and concrete will keep the energy of the wave confined within the concrete tile longer than when concrete tile is in direct contact with the sand.

A sketch of the test scenarios can be seen in figure 3.5.

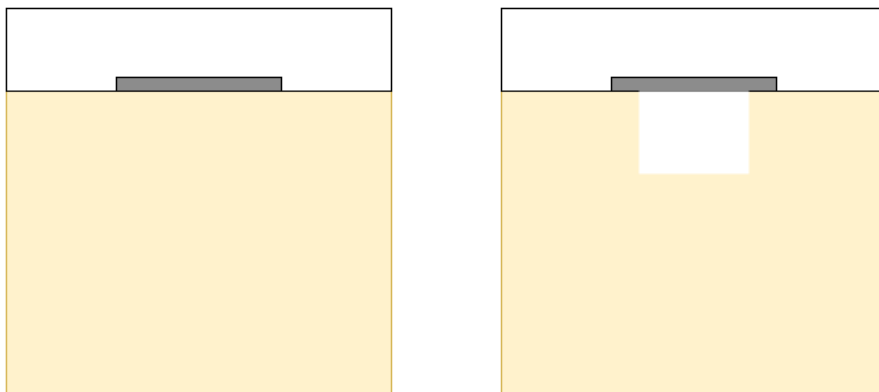


**Figure 3.5:** Test scenarios - undamaged substrate(left) and damaged substrate(right)

### 3.3 Method

#### 3.3.1 Measurement procedure

The measurements are going to be performed under two different scenarios as mentioned in the previous section. First, the concrete tile will be placed on a substrate of sand. The steel ball will be dropped from a certain height, will hit the concrete surface once and then will be caught. In the meantime, the response of the concrete tile will be recorded. Second, sand will be removed from underneath the concrete tile, creating a cavity in the substrate and the measurement is repeated. As reported by Kang et al. (6), the difference between an undamaged substrate(no cavity) and a damaged one(with cavity) it is better represented when the sand is wet. To avoid any possible mismatch between different measurements, the sand was wetted until saturation was reached. The sand is saturated with water when at the bottom of the container that accommodates the sand, a very thin layer of water is present.

To ensure uniformity across all tests, it is preferred that the steel ball will be dropped at the same distance from the sensor. A simple mechanism consisting of a funnel was designed such that this requirement was fulfilled. The force that the ball hits the surface determines the amplitude of the stress waves generated and so, the height at which the ball is going to be dropped will be adjustable. However, as stated in chapter 2, because the spread of the frequencies over time will be analyzed, it is necessary that the height must remain the same while performing measurements with the same sensor.

#### 3.3.2 Data analysis

Data will be collected using the previously mentioned oscilloscope in section 3.1. Before any processing is done, the SNR will be computed using all the measurements and computing the ratio of their summed squared magnitude to that of the noise. The SNR is plotted then using a bar graph and compared among all the sensors. Afterwards, the data is downsampled in order to reduce the computing power that is needed for filtering and so, the order of the filter. As described in section 2.2, all the data will be normalized such that a common scale is reached. It is important that the data is normalized in amplitude because the temporal trace of the thickness frequency is needed. In order to identify the thickness frequency the FFT will be computed for each measurement. The ability of the sensors to identify the same thickness frequency across ten consecutive measurements is assessed and is referred to as its consistency. However, only computing the FFT is not sufficient to assess the state of the substrate on which the tile lays. For this, Short Time Fourier Transform is needed. The data will be split into smaller sections and the FFT will be computed for each section. Sections can overlap to each other and the bigger the overlap, the better the time resolution it becomes. The STFT will be plotted against time in a spectrogram. Next, the trace that has the maximum absolute amplitude is extracted from the STFT. This will result in a row vector which will be also plotted against time. Lastly, the cumulative sum of all the point of each trace is computed and plotted. For longer temporal decays of the excited waves the cumulative sum increases faster than for shorter ones. Thus, the cumulative sum reaches 90% of its maximum amplitude faster for a longer temporal trace than for a shorter one. In this way, the damaged substrate can be distinguished from the undamaged one.

## 4 Results and discussion

In total, 70 measurements have been carried out: 10 for each test scenario for the contactless sensors and 5 for each scenario for the accelerometer. Only a representative figure will be presented for each sensor and test scenario

### 4.1 Time domain response

As mentioned in section 2.1.2, the time evolution of the waves yields to a good characterization of the substrate underneath a concrete tile. The normalized time response of each sensor under the two test scenarios is illustrated in figures 4.1, 4.2, 4.3 and 4.4. Except for the microphone and the accelerometer, the other two sensors do not present a visible difference between a damaged and an undamaged substrate while the data is represented in time domain. Therefore it is necessary to move forward and analyze the response in frequency domain. It is worth mentioning that in figure 4.3 right, the extra noise compared to the measurement taken on the left it is due to the laser beam not being perfectly focused.

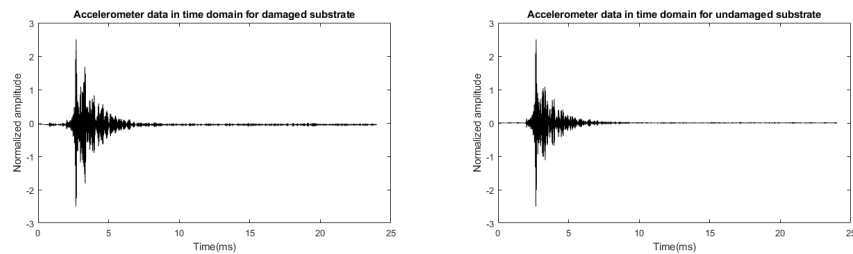


**Figure 4.1:** Accelerometer time response - damaged substrate(left) and undamaged substrate(right)

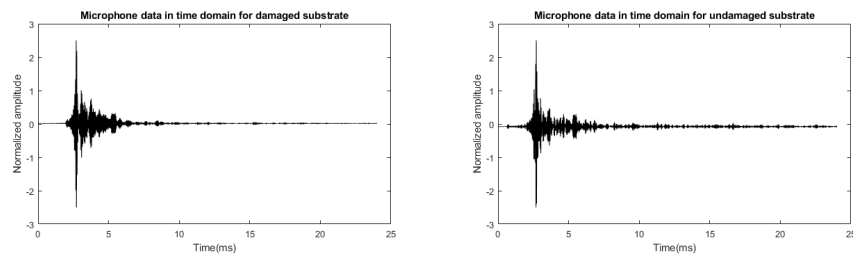


**Figure 4.2:** Microphone time response - damaged substrate(left) and undamaged substrate(right)

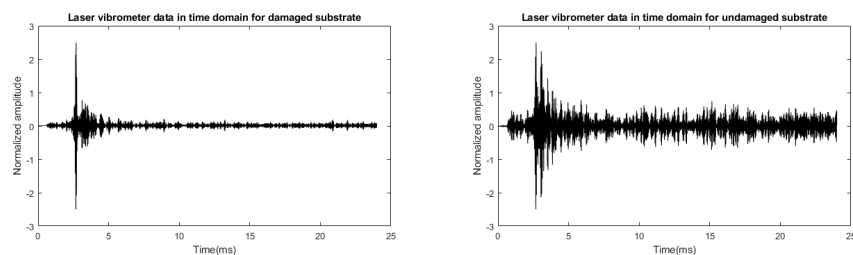


**Figure 4.3:** Laser vibrometer time response - damaged substrate(left) and undamaged substrate(right)

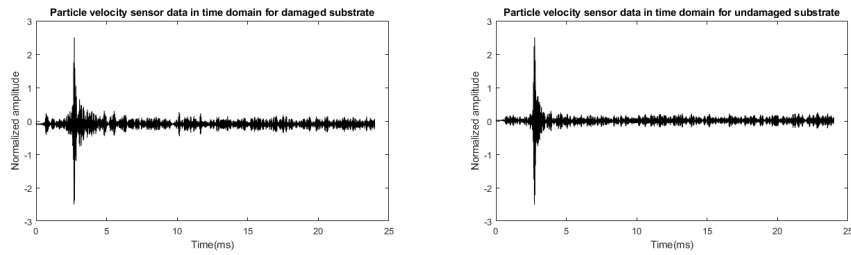


**Figure 4.4:** Particle velocity sensor time response - damaged substrate(left) and undamaged substrate(right)

## 4.2 Signal to noise ratio

Before proceeding to frequency domain analysis, one important parameter that can aid the decision making process about the most suitable sensor for the in-pipe robot is the SNR. For each individual measurement the SNR of each sensor (with respect to the noise recorded beforehand) has been computed and can be seen in figure 4.5. It is noticeable how well the microphone distinguishes itself among other sensors, having the highest SNR values when compared to the contactless sensors. Due to the fact that the accelerometer is directly attached to the surface, it has therefore the highest SNR among all sensors.

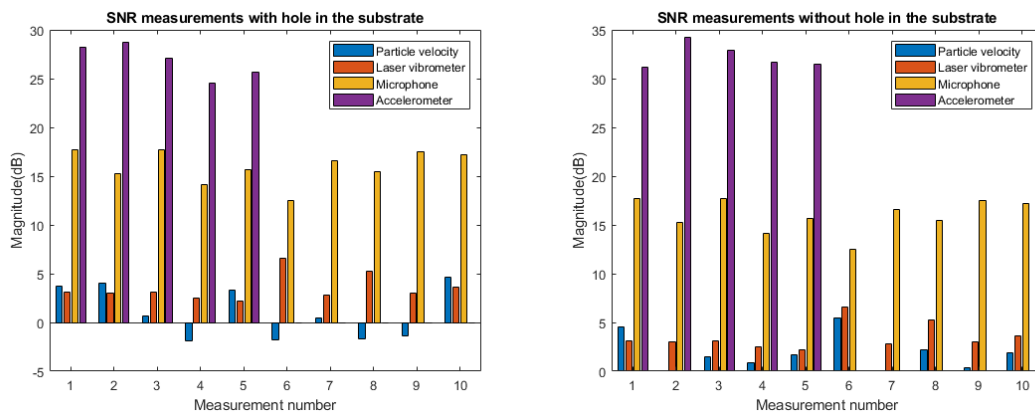


**Figure 4.5:** SNR for all ten measurements for each sensor - damaged substrate(left) and undamaged substrate(right)

The mean value among all 10 measurements has been calculated and presented in figure 4.6. Among all contactless sensors, the microphone ranks highest with a mean SNR of 15.98dB for the test scenario with an undamaged substrate and 19.05dB for the test scenario with a damaged substrate.

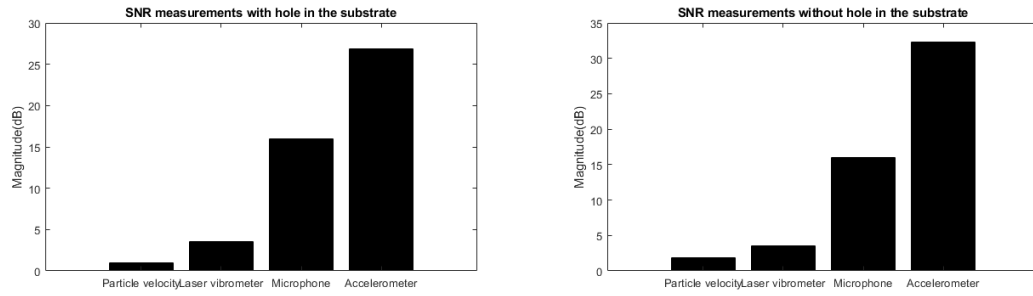


**Figure 4.6:** Average SNR for each sensor - damaged substrate(left) and undamaged substrate(right)

### 4.3 Frequency spectrum using FFT

The frequency spectrum of the signal was analyzed using the Fast Fourier Transform in order to identify the thickness frequency. Before computing the FFT, the signal was downsampled by a ratio of 10. Afterwards the signal is filtered using an FIR bandpass filter with with the bandpass starting at 19.7kHz and ending at 30kHz. The response of the filter can be seen in figure 4.7.

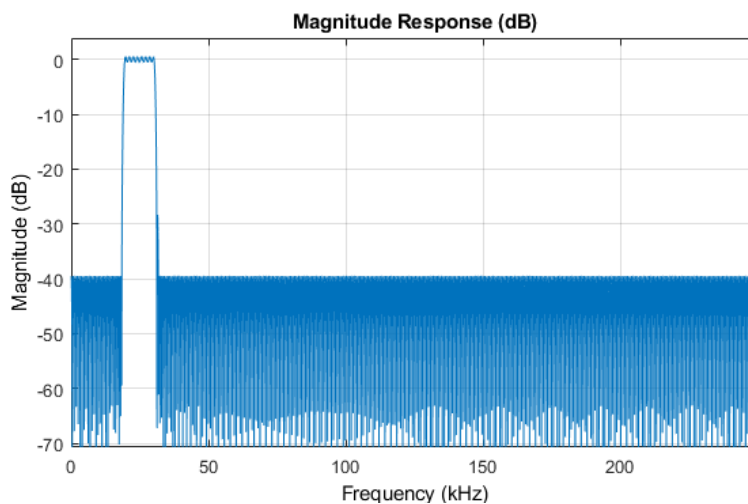


**Figure 4.7:** Bandpass filter response

The thickness frequency has been identified by finding the maximum absolute amplitude available in the frequency spectrum. The results of all the measurements can be seen in figures 4.8, 4.9, 4.10 and 4.11.

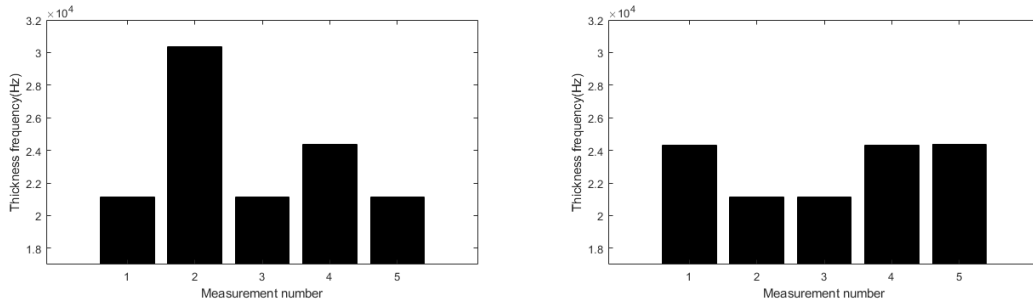


**Figure 4.8:** Thickness frequency for accelerometer - damaged substrate(left) and undamaged substrate(right)

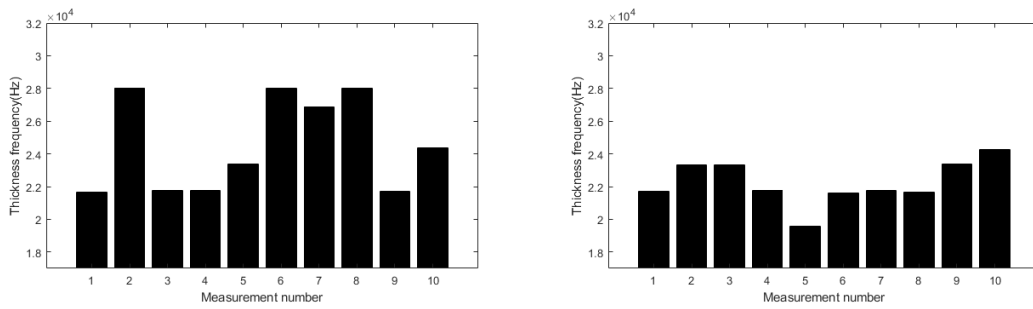


**Figure 4.9:** Thickness frequency for laser vibrometer - damaged substrate(left) and undamaged substrate(right)

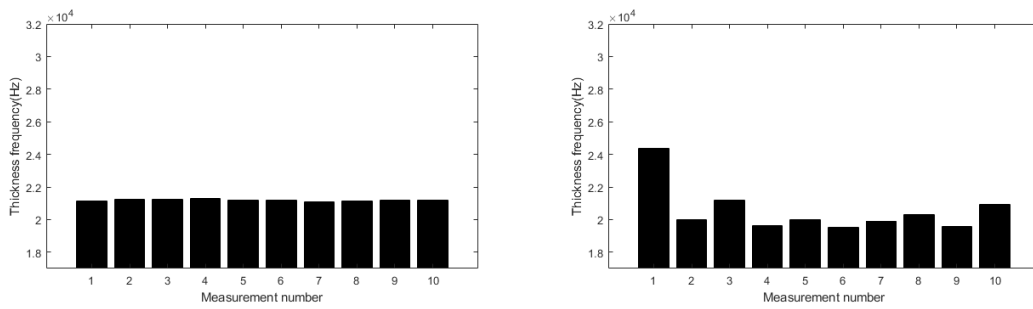


**Figure 4.10:** Thickness frequency for microphone - damaged substrate(left) and undamaged substrate(right)

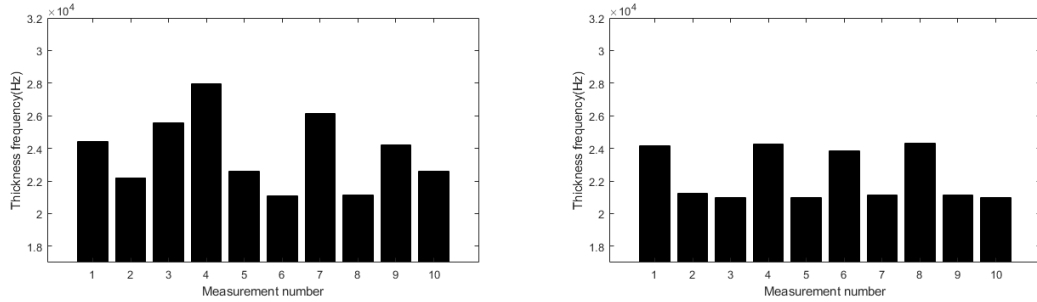


**Figure 4.11:** Thickness frequency for particle velocity sensor - damaged substrate(left) and undamaged substrate(right)

The standard deviation has been computed for all measurements. For the scenario where the substrate was damaged, the microphone shows the lowest standard deviation of 65.29Hz. For the scenario where the substrate is undamaged, the laser vibrometer displays the lowest standard deviation of 1.34kHz, followed by the microphone with a standard deviation of 1.45kHz. The complete results can be seen in table 4.1.

Sensor	Standard deviation(Hz)	
	Undamaged substrate	Damaged substrate
Accelerometer	1.76e+03	4.02e+03
Particle velocity sensor	1.59e+03	2.26e+03
Laser vibrometer	1.34e+03	2.89e+03
Microphone	1.45e+03	65.29

**Table 4.1:** Standard deviation thickness frequency

#### 4.4 Time development of thickness frequency using STFT

Lastly, the sensors were assessed based on how good they can differentiate between a damaged substrate and an undamaged one. According to section 2.1.2, the temporal trace of the frequencies should last longer for a damaged substrate, since the wave is reflected back inside the concrete tile, and shorter for the undamaged one. First, the Short Time Fourier Transform has been plotted and can be seen in figures 4.12, 4.13, 4.14 and 4.15. Compared to the time domain representation, the STFT plots show a better difference in magnitude over time for both scenarios where the substrate is damaged and undamaged. This applies for all the sensors tested.

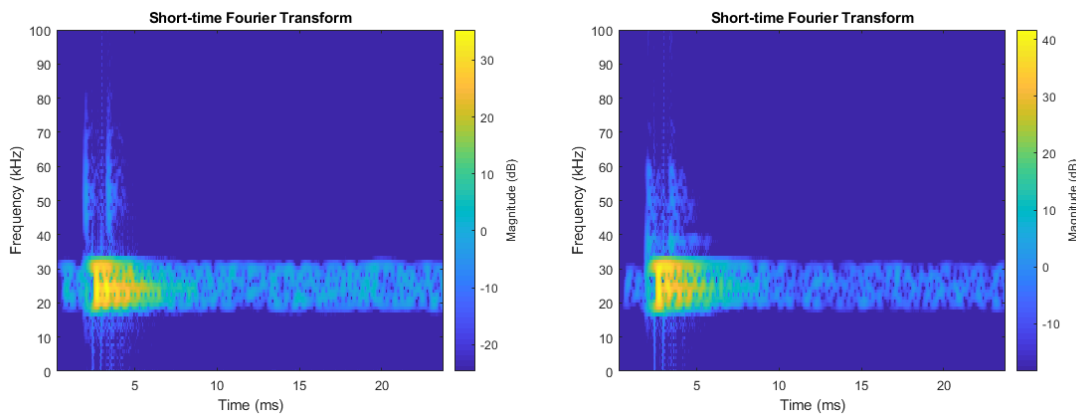


**Figure 4.12:** STFT accelerometer - damaged substrate(left) and undamaged substrate(right)

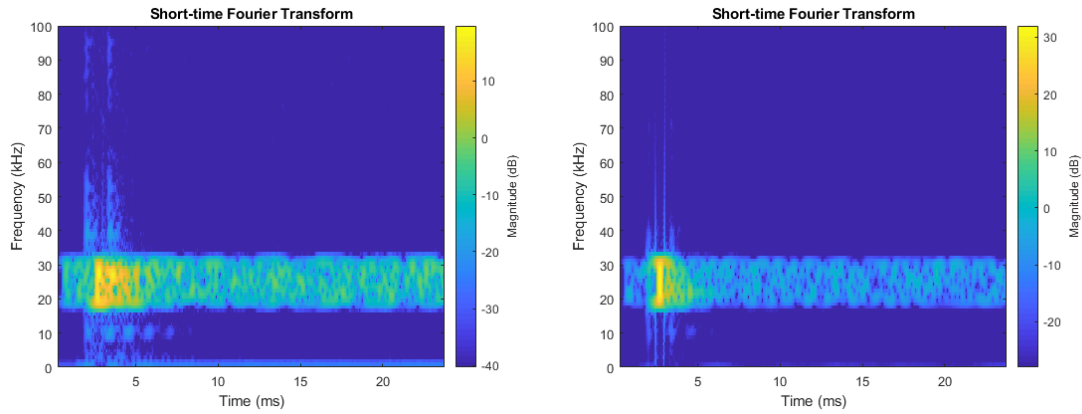


**Figure 4.13:** STFT laser vibrometer - damaged substrate(left) and undamaged substrate(right)

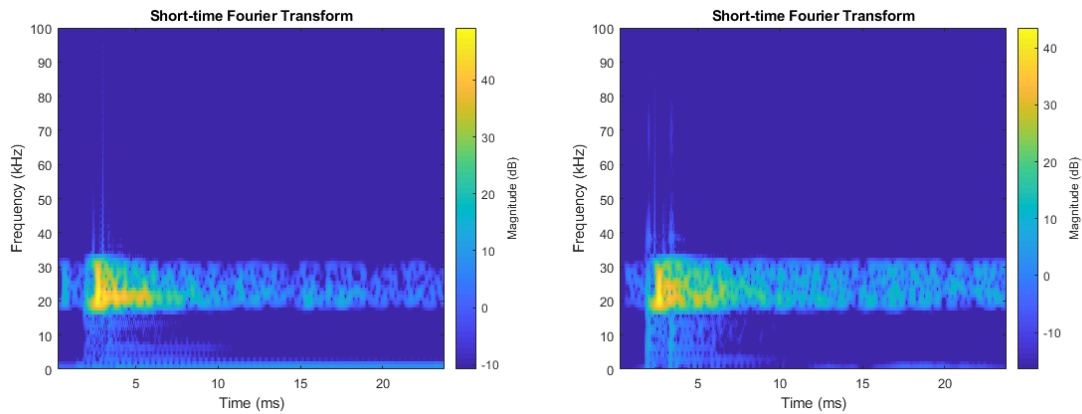


**Figure 4.14:** STFT microphone - damaged substrate(left) and undamaged substrate(right)

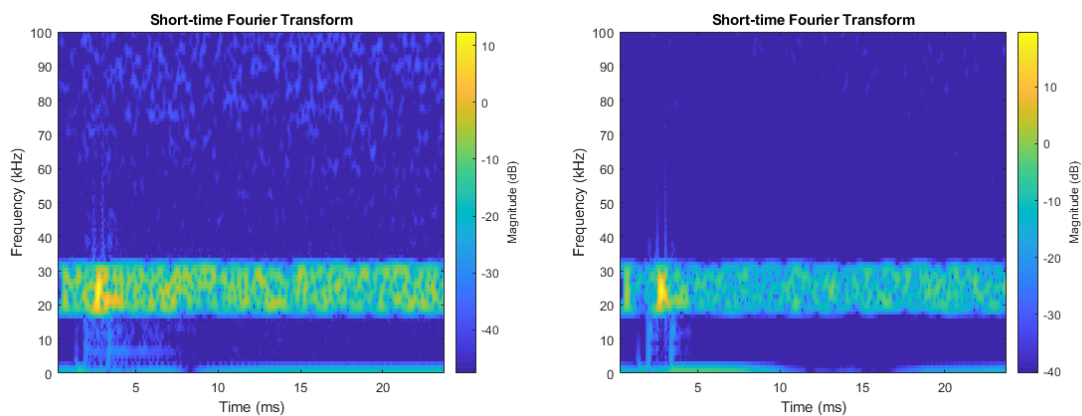


**Figure 4.15:** STFT particle velocity sensor - damaged substrate(left) and undamaged substrate(right)

Furthermore, the trace with the highest magnitude at each instance of time has been isolated and analyzed. The cumulative sum of all the points has been computed and the point at which it reaches 90% of its maximum has been found. For a longer temporal trace, the cumulative sum reaches 90% of its maximum amplitude faster than for a shorter temporal trace, thus showing

the difference between a damaged substrate and an undamaged one. This can be seen in figures 4.16, 4.17, 4.18 and 4.19. For a fair comparison, all curves have been normalized.

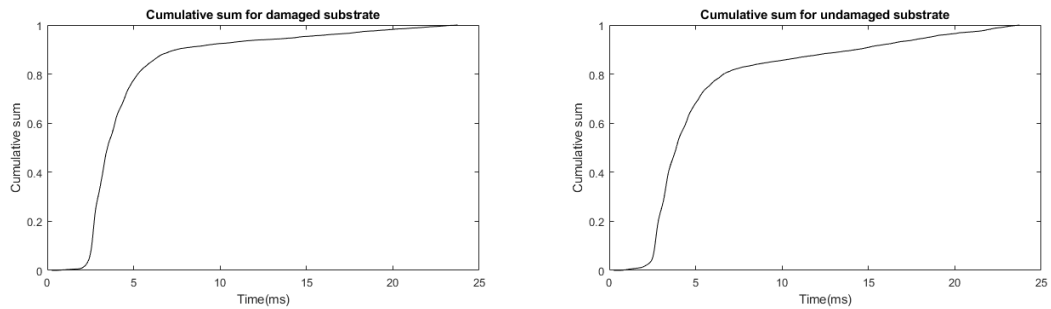


**Figure 4.16:** Cumulative sum accelerometer - damaged substrate(left) and undamaged substrate(right)

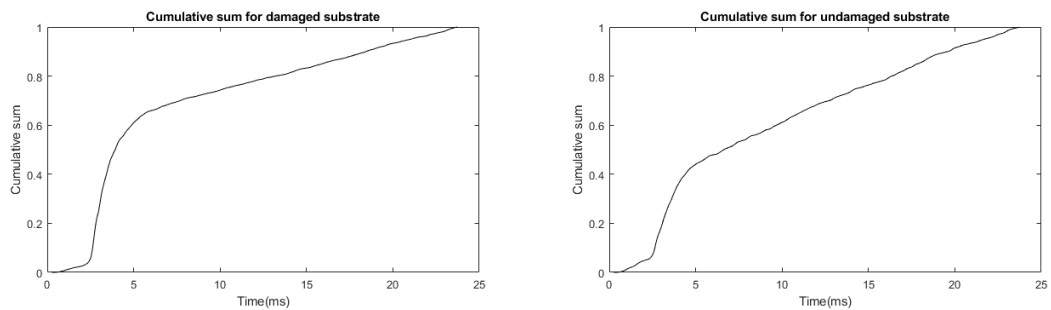


**Figure 4.17:** Cumulative sum laser vibrometer - damaged substrate(left) and undamaged substrate(right)

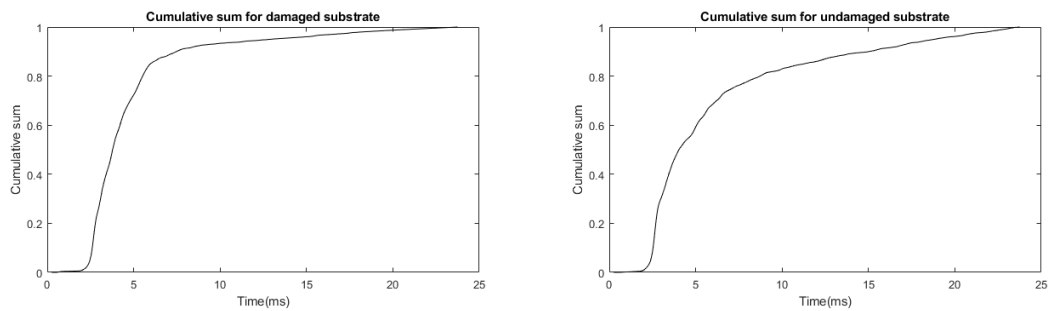


**Figure 4.18:** Cumulative sum microphone - damaged substrate(left) and undamaged substrate(right)

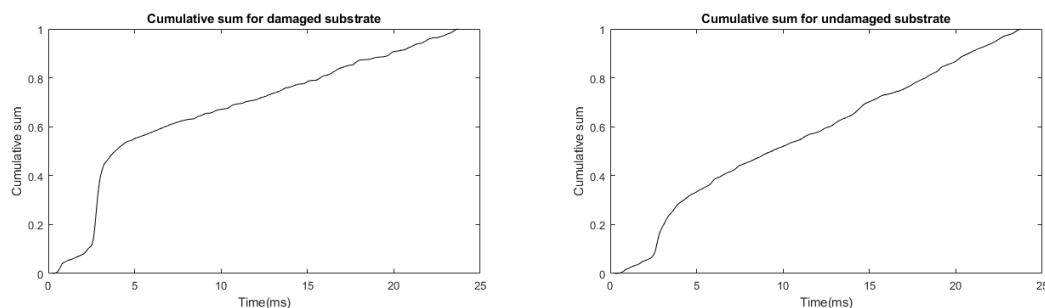


**Figure 4.19:** Cumulative sum particle velocity sensor - damaged substrate(left) and undamaged substrate(right)

The points in time at which the cumulative sum reaches 90% of its maximum amplitude can be seen in table 4.2. The table contains the results of all 70 measurement.

Sensor	Substrate state	Point in time when cumulative sum reaches 90% of its maximum(ms)										Average
		1	2	3	4	5	6	7	8	9	10	
Accelerometer	Damaged	6.68	6.20	6.94	10.78	7.52	-	-	-	-	-	7.62
	Undamaged	7.4880	8.4480	7.7440	7.2640	14.3040	-	-	-	-	-	9.04
Laser vibrometer	Damaged	17.66	19.00	18.46	20.03	20.16	19.80	20.16	18.04	19.16	19.93	19.224
	Undamaged	20.73	19.71	19.58	21.21	20.38	18.01	20.22	18.43	20.16	20.19	19.86
Microphone	Damaged	6.75	7.52	7.48	8.48	7.90	7.52	7.00	6.40	7.36	7.32	7.37
	Undamaged	12.25	14.46	15.04	14.97	13.08	15.32	14.33	9.66	12.64	13.44	13.52
Particle velocity sensor	Damaged	20.00	19.84	21.40	20.48	19.96	20.96	19.26	20.57	20.03	18.36	20.08
	Undamaged	20.12	20.73	20.12	21.28	20.54	20.32	21.05	19.58	21.15	21.12	20.60

**Table 4.2:** Points in time at which the cumulative sum reaches 90% of its maximum amplitude for all 70 measurements

A difference ratio has been computed on average for each sensor. It is the ratio between the point at which the cumulative sum reaches 90% of its maximum amplitude when the substrate is undamaged and when the substrate is damaged. If the ratio is higher than one, the sensor is able to distinguish the difference, if the ratio is lower than one, the sensor is not able to distinguish the difference between the two test scenarios. It can be seen from table 4.3 that the microphone has the best difference ratio of 1.86.

Sensor	Difference ratio
Accelerometer	1.192
Particle velocity sensor	1.026
Laser vibrometer	1.033
Microphone	1.86

**Table 4.3:** Mean difference ratio - the higher the better

## 5 Conclusion and recommendations

### 5.1 Conclusion

*How is a void under a concrete plate discovered using impact-echo method?*

An impact at the surface of a concrete tile generates stress waves within the material. The frequency of the primary waves is proportional to the thickness of the concrete sample. It was expected that at the interface between concrete and wet sand (substrate without a void), the waves are partially absorbed by the substrate, thus decaying faster over time. In contrast, at the interface between concrete and air (sand substrate containing a void), the waves are reflected back into the concrete plate, thus decaying slower over time. It has been shown both through literature review and experiments that due to different specific acoustic impedance between wet sand and air, a void underneath a concrete tile can be discovered by analyzing the temporal trace of the excited waves. It can be concluded that impact-echo method can be successfully used to assess the state of the substrate underneath a concrete plate.

*How do material properties (density and Poisson's ratio) of the concrete tile affect the impact-echo response?*

Literature review revealed that the density of the concrete and Poisson's ratio affect the thickness frequency. Calculations have been performed for a concrete tile with a thickness of 80 mm. It has been shown that the thickness frequency increases linearly with an increase of Poisson's ratio and will decrease linearly with an increase in the density of the concrete.

*How can the measured data be processed to determine the presence of a flaw in the support substrate, underneath the concrete plates?*

Both literature review and experiments proved that the key element for assessing the state of the substrate is to analyze the data in frequency domain. Using Short Time Fourier Transform, the evolution of the excited waves over time was analyzed. From this data, the temporal trace that has maximum absolute amplitude has been followed and plotted. For a damaged substrate, the trace presents a slower decay than for an undamaged one. A cumulative sum was computed for each repetition of the measurement. For a slower decay, the cumulative sum increases faster than for a faster decay. As a final step, a ratio between how fast the cumulative sum reaches 90% of its maximum amplitude when the substrate is damaged and when the substrate is not damaged has been computed. It has been concluded that following this interpretation of the data, a damaged substrate can be distinguished from an undamaged one.

*How do sensors compare to each other for the detection of the impact-echo response and the state of the substrate?*

Overall, all sensors were able to identify the thickness frequency and to distinguish between a damaged and an undamaged substrate. Regarding the thickness frequency, the accelerometer proved to have the highest standard deviation with an average of 2.89 kHz while the microphone had the lowest standard deviation of 757.64 Hz on average. Furthermore, the microphone has also the highest difference ratio, which proves that it can distinguish between a damaged and an undamaged substrate better than the other three sensors.

To conclude, it is advised that the microphone would be the most suitable sensor to be mounted on an in-pipe inspection robot. First, it has the highest SNR, averaging 17.5 dB. Second, it has the lowest standard deviation on average of 757.64 Hz which gives it a great advantage compared to the other sensors. Lastly, it has the highest difference ratio of 1.86 which obsoletes the other sensors analyzed.

## 5.2 Future work

For the purpose of this thesis, the response of the sensors was investigated under laboratory conditions. In the future, the research can be taken one step further and the sensors should be investigated in an environment as close as possible to a real life scenario. Furthermore, due to the bandwidth limitations of the sensors, only a concrete tile with a specific thickness of 80mm was used, however, the research can be extended to thinner tiles as well. In order to excite the thickness frequency, a free falling steel ball was used. To improve the quality of the experiment, a dedicated impactor that provides a high level of consistency and accuracy can be used. Furthermore, different concrete mixtures and substrate mixtures can be tested as well as different void sizes.

---

## A Appendix 1

There are two main MATLAB codes that have been used for this research report. First one is called *Ball\_Size*. It is used to compute the the graphs regarding the thickness frequency presented in section 2.1. Simply running the code will plot 3 different graphs.

PLEASE RUN THIS CODE SECTION BY SECTION AND NOT ALL AT ONCE! Second MATLAB code is divided in multiple subsections as it follows:

- Initial parameters - initial parameters are defined
- Screen& figures - screen information is retrieved to center figures
- Import data and clean other variables - import data from a folder that has to added to path; if the variables exist, the program won't load them again as it takes time
- SNR calculation and plot - calculates SNR and plots values for individual measurements and average/sensor
- Downsample and filter - downsample the data by a downsampling factor mentioned in section *Initial parameters*
- Normalize data - amplitude normalization of data; it is necessary to to run this section if you want to see the data represented in time domain on the same scale
- Plot signals in time domain - plot the signals in time domain, after the data was normalized
- FFT accelerometer - computes the single sided FFT and displays it alongside with the thickness frequency
- FFT particle velocity sensor - computes the single sided FFT and displays it alongside with the thickness frequency
- FFT laser vibrometer - computes the single sided FFT and displays it alongside with the thickness frequency
- FFT microphone - computes the single sided FFT and displays it alongside with the thickness frequency
- Short time fourier transform - computes the short time Fourier transform; plots the cumulative sum for each repetition of the experiment; plots the difference ratio

It is essential to run the first 3 section such that the program obtains all the input data. Normalize data should not be run unless the time domain representation is necessary. This is due to the fact that the data is normalized after computing the FFT and STFT

## Bibliography

- [1] Behringer (2000), Piezoelectric Charge Accelerometer Types 4374 and 4374-L.  
[https://downloads.music-group.com/software/behringer/ECM8000/ECM8000\\_C\\_Specs.pdf](https://downloads.music-group.com/software/behringer/ECM8000/ECM8000_C_Specs.pdf)
- [2] Brüel & Kjær (2018), Piezoelectric Charge Accelerometer Types 4374 and 4374-L.  
<https://www.bksv.com/-/media/literature/Product-Data/bp2038.ashx>
- [3] Carino, N. J. et al. (2001), The impact-echo method: an overview, in *Proceedings of the 2001 Structures Congress & Exposition*, American Society of Civil Engineers, pp. 21–23.
- [4] Colla, C. and R. Lausch (2003), Influence of source frequency on impact-echo data quality for testing concrete structures, **vol. 36**, no.4, pp. 203–213.
- [5] Dorf and Richard (1990), *Engineering handbook*, Springer-Verlag Berlin Heidelberg GmbH.
- [6] Kang, J. M., S. Song, D. Park and C. Choi (2017), Detection of cavities around concrete sewage pipelines using impact-echo method, *Tunnelling and Underground Space Technology*, **vol. 65**, pp. 1–11.
- [7] Krautkrämer, J. and H. Krautkrämer (1990), *Ultrasonic testing of materials*, Springer-Verlag Berlin Heidelberg GmbH.
- [8] Lin, J.-M. and M. Sansalone (1997), A procedure for determining P-wave speed in concrete for use in Impact-Echo Testing using a Rayleigh wave speed measurement technique, *Special Publication*, **vol. 168**, pp. 137–166.
- [Microflown Technologies] Microflown Technologies (), The Microflown.  
<https://www.microflown.com/>
- [10] Polytec (2018), OFV-5000 Vibrometer Controller.  
<https://www.polytec.com/eu/vibrometry/products/single-point-vibrometers/ofv-5000-modular-vibrometer/>
- [11] Ryden, N., M. J. Lowe and P. Cawley (2008), NON-CONTACT SURFACE WAVE SCANNING OF PAVEMENTS USING A ROLLING MICROPHONE ARRAY, in *AIP Conference Proceedings*, volume 975, AIP, pp. 1328–1332.
- [12] Sansalone, M. (1997), Impact-echo: the complete story, **vol. 94**, no.6, pp. 777–786.
- [13] Zhu, J. and J. S. Popovics (2007), Imaging concrete structures using air-coupled impact-echo, **vol. 133**, no.6, pp. 628–640.